Applied Catalysis B: Environmental 90 (2009) 242–248

Contents lists available at ScienceDirect

Applied Catalysis B: Environmental

journal homepage: www.elsevier.com/locate/apcatb

Silicon nanowire/TiO_2 heterojunction arrays for effective photoelectrocatalysis under simulated solar light irradiation

Hongtao Yu, Shuo Chen, Xie Quan *, Huimin Zhao, Yaobin Zhang

School of Environmental and Biological Science and Technology, Key Laboratory of Industrial Ecology and Environmental Engineering (Ministry of Education, China), Dalian University of Technology, Dalian 116024, China

ARTICLE INFO

Article history:
Received 16 November 2008
Received in revised form 22 February 2009
Accepted 5 March 2009
Available online 19 March 2009

Keywords:
Silicon nanowire (SiNW)
TiO_2
Photoelectrocatalysis
Heterojunction

ABSTRACT

The silicon nanowire (SiNW)/TiO_2 heterojunction arrays have been prepared by chemical vapor depositing a TiO_2 layer on SiNW arrays which are obtained by chemical etching of Si wafers. The types of SiNW/TiO_2 heterojunctions can be modulated simply by using p-type or n-type Si wafers. Compared with samples of depositing TiO_2 on p-type or n-type Si wafers (p-Si/TiO_2 or p-Si/TiO_2), both n-SiNW/TiO_2 and p-SiNW/TiO_2 heterojunctions can improve the ultraviolet photoresponse under a bias potential, and in particular, a remarkable visible photoresponse of n-SiNW/TiO_2 heterojunction is observed when the bias potential is higher than 1.7 V (vs. SCE). Cyclic voltammetry (CV) curves illuminate that n-SiNW/TiO_2 heterojunctions have steady visible photoresponse in aqueous solution. According to the surface photovoltage (SPV) measurements, it is found that n-SiNW/TiO_2 heterojunctions possess window effect, namely, n-SiNW/TiO_2 heterojunctions can utilize the superposition photoresponse in the wavelength ranges from 300 to 400 nm (contributed by TiO_2) and from 400 to 800 nm (contributed by n-SiNW). The mechanism of this phenomenon is explained based on the energy band model. The photoelectrocatalytic activity of the n-SiNW/TiO_2 heterojunction arrays is evaluated using phenol as a test substance under Xe lamp irradiation. The kinetic constant and total organic carbon (TOC) removal are 1.7 times and 2 times as great as those of n-Si/TiO_2, respectively.

1. Introduction

Photocatalysis, as a useful technique in environmental cleaning, can degrade a wide range of contaminants in air or water rapidly and drastically [1]. In the photocatalytic process in water, photocatalysts are generally loaded on the surface of carriers to avoid the difficulties of separating suspended TiO_2 particles from aqueous solution as well as enhance quantum efficiency by applying a bias potential on the conductive carriers [2]. Among these carriers, conductive silicon wafer is the most attractive one, because the lower crystallization temperature [3,4] and faster phase transformation rate [5] of TiO_2 can be obtained using silicon substrate than using other materials, and at the same time, the contaminants of TiO_2 by component of carrier can be suppressed by using silicon substrate [6]. Therefore, many groups select silicon wafer as carrier of TiO_2 [7–10], and the effects of conductive types [11,12], crystal face [13] or surface morphology [14–16] of silicon wafers on the properties of TiO_2 are also investigated. Besides silicon wafer, nano-silicon [17] and porous silicon [18] are also used to support TiO_2. Compared with bulk or disorder nano-carriers, aligned nano-materials are regarded as better carriers because they possess large specific surface area and can be constructed with TiO_2 to form heterojunction with the photogenerated charge separation ability [19,20]. However, the work on using nano-silicon array as carrier of photocatalysts is rather limited.

The blank would be filled up since silicon nanowire (SiNW) arrays have been fabricated [21]. SiNW as a novel material has been studied extensively because of its high compatibility with standard CMOS technology and possible integration in future electronic devices. Because SiNW has considerable photo-harvesting ability [22] and its conductive types can be modulated [23], it is a promising material to construct various types of heterojunctions with semiconductor photocatalysts. And subsequently, it is favorable to explore other properties of heterojunctions in photocatalytic degradation of pollutant, such as window effect, which is a common concept in physics of semiconductors [24] and has been widely investigated in solar cells [25–29] and solar light water splitting [30–32]. When a heterojunction, which is constructed by covering a wide band-gap semiconductor (such as TiO_2) on the top surface of a narrow band-gap semiconductor, is illuminated with solar light, the UV light could be absorbed by TiO_2, while the visible light could permeate the TiO_2 layer on the top of the heterojunction and would be absorbed by the narrow-gap semiconductor in the bottom of the heterojunction. Because the short and long wavelength lights can be absorbed by

* Corresponding author. Tel.: +86 411 84706140; fax: +86 411 84706263.
E-mail address: quanxie@dlut.edu.cn (X. Quan).

0926-3373/$ – see front matter © 2009 Elsevier B.V. All rights reserved.
doi:10.1016/j.apcatb.2009.03.010

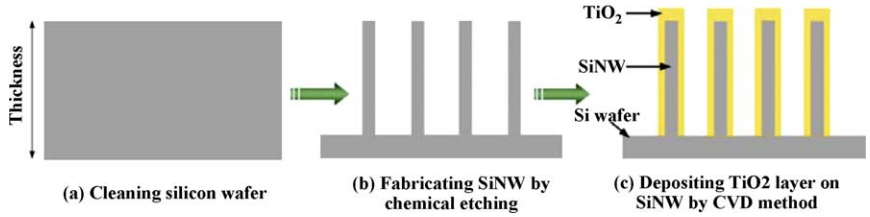

Fig. 1. Schematic diagram of the fabrication process of SiNW/TiO_2 heterojunction array.

TiO_2 and the narrow-gap semiconductor, respectively, the photoconversion efficiency is enhanced effectively. In this process, TiO_2 acts as a window of narrow-gap semiconductor, so this property of heterojunction is named window effect. Due to window effect, the heterojunction photocatalyst can utilize both visible light and UV light of the solar spectrum in photocatalytic process, and thus its photocatalytic ability would be enhanced remarkably. However, no papers to date have been published on window effect in photocatalytic degradation of pollutant.

It has higher requests for photocatalytic electrodes in degradation of pollutant than in solar cells or solar light water splitting. The photoelectrodes in degradation of pollutant must be composed of nontoxic materials, be stable with respect to photocorrosion, have band-gap energies sufficient for degradation of pollutant and have a high efficiency in general electrolyte. In all these aspects, the SiNW/TiO_2 heterojunction arrays would be a proper electrode. Furthermore, most photocatalytic electrodes (existing in the domain of solar cell or water splitting) with window effect are the planar multilayer structure [33], while the SiNW/TiO_2 heterojunction arrays are the aligned coaxial-cable structure. It is obvious that the SiNW/TiO_2 heterojunction arrays possess high specific surface areas, enhanced antireflection ability and excellent transfer routes for charge carriers.

Herein, we fabricate the SiNW/TiO_2 heterojunction arrays on conducting silicon substrate. By using p-type or n-type silicon wafers, p-SiNW and n-SiNW can be obtained, and subsequently, p–n and n–n heterojunctions of SiNW/TiO_2 are fabricated. It is found that the n–n junction has window effect, but p–n junction not. Because n-SiNW/TiO_2 can response to both visible light and UV light of the solar spectrum, its photocatalytic mineralizing ability is enhanced.

2. Experimental methods

2.1. Fabrication of SiNW/TiO_2 heterojunction arrays

Si wafers (n-type Si (1 1 1), phosphorus-doped, and p-type Si (1 1 1), boron-doped) were purchased from China Electronics Science & Technology Group No. 46 Institute. The process of cleaning Si wafers involved firstly rinsing in ultrasonic bath with acetone (5 min), ethanol (5 min) and deionized water (10 min), sequentially; secondly chemical etching by immersing in a mixture of H_2SO_4 and H_2O_2 (3:1 in volume) for 30 min; and lastly dipping into a solution of HF (5%) for 1 min and drying in argon flow at room temperature.

The clean Si wafer was then put into the vessel containing the etching solution of 4.6 M HF and 0.02 M $AgNO_3$ [21]. The reaction was lasted for 60 min at 50 °C in thermostatic water bath. After reaction, the sample was put into the mixture of HNO_3 and H_2O (1:1 in volume) to remove Ag catalysts. Then the SiNW array was dipped into 5% HF solution for 1 min. As soon as the SiNW array was taken out, it was rinsed with water immediately, dried in a Ar flow, put into a tubular quartz reactor in a furnace and then heated in a combined flow of Ar (800 mL min^{-1}) and H_2 (100 mL min^{-1}). When the temperature reached 320 °C, the H_2 flow was turned off and titanium (IV) isopropoxide (TTIP) was fed continuously into the tubular quartz reactor through a capillary. At the outlet of the capillary, TTIP was immediately volatilized and swept into the reaction zone by the Ar flow. After 10 min, the reaction finished and the substrate was annealed in air at 400 °C for 60 min with a heating rate of 2 °C min^{-1}. Then the substrate was allowed to cool to room temperature, and SiNW/TiO_2 heterojunction was obtained. Schematic diagram of this fabrication process was shown as Fig. 1, and the flow chart was in Supplementary Material. As comparison, TiO_2 was deposited on the clean Si wafers to fabricate Si/TiO_2. If the Si wafer was p type, p-SiNW/TiO_2 and p-Si/TiO_2 was obtained, while n-SiNW/TiO_2 and n-Si/TiO_2 could be fabricated by using n-type Si wafer.

2.2. Characterization

Environmental scanning electron microscopy (ESEM Quanta 200 FEG) and transmission electron microscopy (TEM FEI-Tecnai G^2 20) coupled with an energy-dispersive X-ray spectrometer (EDX) were employed to characterize the morphologies of SiNW/TiO_2 heterojunctions. The crystallographic structures of the samples were characterized by X-ray diffractometer (XRD; Shimadzu Laboratory X XRD-6000). The photovoltage was measured using a surface photovoltage (SPV) measurement system which consisted of a monochromator (model Omni-k 3005) and a lock-in amplifier (model SR830-DSP) with an optical chopper (model SR540). Photoelectrochemical measurements were preformed in 0.01 M Na_2SO_4 using three-electrode cell that was connected to a CHI 650B electrochemical station (CH Instruments, Shanghai Chenhua, China), where the SiNW/TiO_2 heterojunction arrays acted as the working electrode, a platinum foil as the counter electrode and the SCE as the reference electrode. A high pressure xenon short arc lamp (CHF-XM35-500W, Beijing Changtuo Co., China) was used as the light source to simulate solar light. The light intensity was 100 mW cm^{-2}.

2.3. Photocatalytic experiment

Photocatalytic degradation of phenol in the aqueous solution using 0.01 M Na_2SO_4 as the electrolyte was carried out under the 500 W xenon lamp irradiation in a reactor with a quartz window (1 cm × 1 cm) to allow the incident radiation to enter with minimal attenuation. The n-SiNW/TiO_2 arrays served as the photoanode, a platinum foil and the SCE acted as the counter electrode and the reference electrode, respectively. For comparison, the n-Si/TiO_2 was used as the photoanode by replacing the n-SiNW/TiO_2 arrays. The applied areas of the n-SiNW/TiO_2 and the n-Si/TiO_2 are both 1 cm × 1 cm. The concentration of phenol was determined by high performance liquid chromatography (HPLC, Waters 2695, Separations module) with a Sunfire™ C18 (5 μm) reverse-phase column at 30 °C equipped with photodiode array detector (Waters 2996). The mobile phase was 0.5 mL min^{-1} of methanol and water (v:v = 0.55:0.45) and the wavelength was set at 280 nm for phenol and 254 nm for intermediates, respectively. Total organic carbon analyzer (TOC-V_{CPH}, Shimadzu, Japan) was employed for TOC determination.

3. Results and discussion

3.1. Morphologies and crystallographic structures

Fig. 2a illuminates that large-scale oriented high-aspect-ratio n-SiNW arrays can be produced on the surface of Si wafer by immersing it in etching solution for 60 min. After depositing TiO_2 around SiNW, the array structure remains without destruct (Fig. 2b). While depositing TiO_2 on n-Si wafer, the TiO_2 nanoparticles congregate into big ball with the diameter of about 2 μm (Fig. 2c). Fig. 3a is a TEM image of a single SiNW. Its diameter is about 200 nm, which enlarges to about 400 nm after depositing TiO_2, and there are clear boundaries between SiNW core and TiO_2 shell (inset in Fig. 3a). Fig. 3b is the EDX analysis, which shows that the synthesized products contain Si, Ti and O elements (Cu signals are from copper TEM grid) and the element ratio of Ti and O is about 1:2, that is, the shell layer is composed of TiO_2. Fig. 3c is a high-magnified TEM image of TiO_2 shell layer, from which the

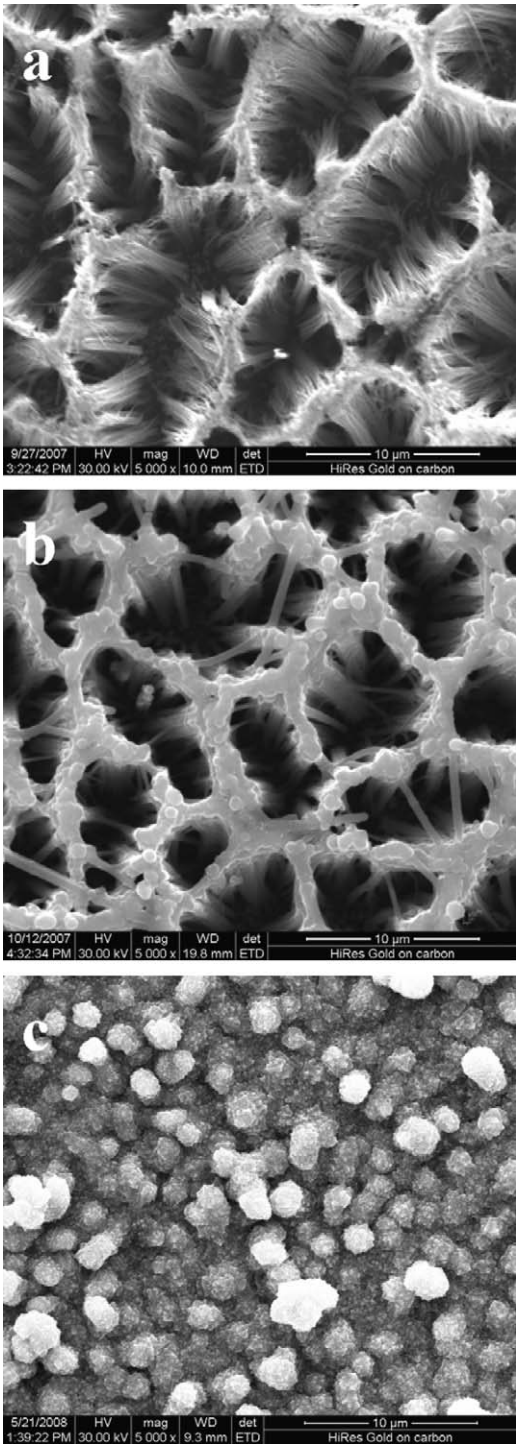

Fig. 2. SEM images of SiNW (a), SiNW/TiO_2 (b) and Si/TiO_2 (c).

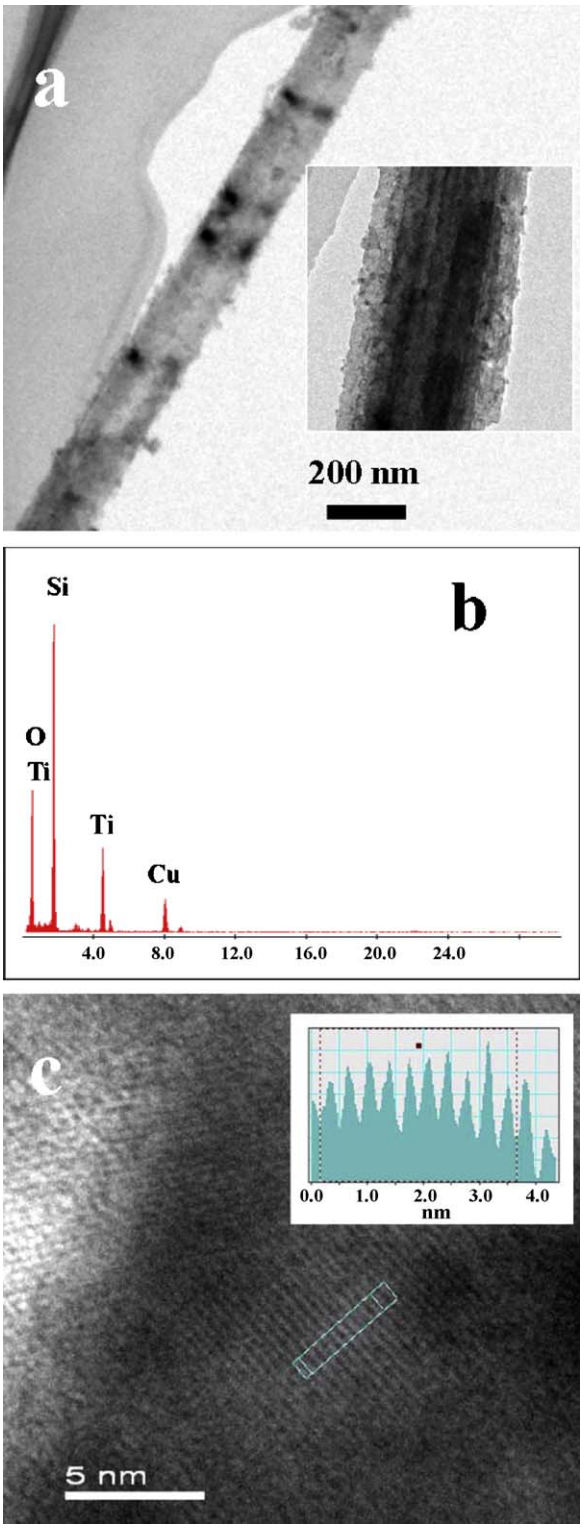

Fig. 3. (a) TEM image of SiNW and the inset is TEM image of SiNW/TiO_2. (b) EDX spectrum of SiNW/TiO_2. (c) HRTEM image of TiO_2 layer around SiNW and the inset is the line profile from the area marked with the rectangular frame.

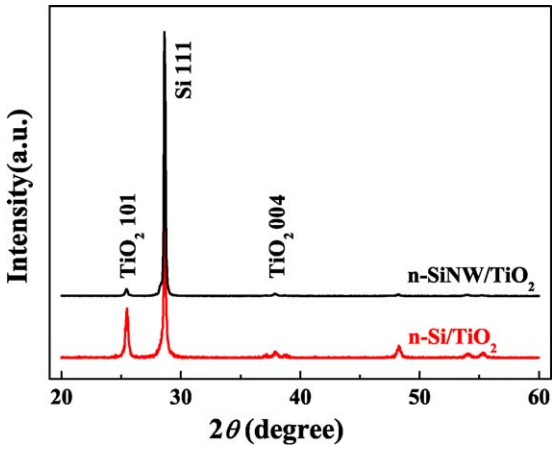

Fig. 4. XRD patterns of n-Si/TiO_2 and n-SiNW/TiO_2.

cubic lattice feature of the edge is clearly visible. In order to obtain the distance between the adjacent lattice fringes, the line profile from the area labeled by the rectangular frame in Fig. 3c is displayed in the inset. As shown in this inset, the periodic fringe spacing of 0.351 nm can be assigned to the interplanar distance of the (1 0 1) plane of anatase TiO_2. In addition, the loading amount of TiO_2 is 0.93 mg cm^{-2} for n-SiNW/TiO_2 by calculating the mass difference of SiNW/TiO_2 and SiNW.

In order to determine crystallographic structures of the samples, XRD patterns of SiNW/TiO_2 and Si/TiO_2 are shown in Fig. 4. The peaks at $2\theta = 25.3^\circ$ and 28.4° correspond to anatase TiO_2 (1 0 1) reflections and Si (1 1 1) reflections, respectively. Moreover, the average diameter of TiO_2 is 31.8 nm for Si/TiO_2 and 25.4 nm for SiNW/TiO_2 according to Scherrer equation [34]. Comparison with Si/TiO_2, the peak locations of SiNW/TiO_2 are the same, but the peak intensities are changed. It is obvious that the specific surface area of SiNW array is larger than that of Si wafer. As a result, the thickness of TiO_2 layer on SiNW array is thinner than that on Si wafer if depositing TiO_2 for the same duration. In this condition, Si diffraction peak of SiNW/TiO_2 is stronger than that of Si/TiO_2, while TiO_2 diffraction peaks of SiNW/TiO_2 are weaker than that of Si/TiO_2.

3.2. Photoelectrochemical properties

The photoelectrochemical measurements of SiNW/TiO_2 heterojunctions are performed in 0.01 M Na_2SO_4 solution. The simulated solar light is provided by the xenon lamp and the visible light is obtained by using a cutoff filter, which allows wavelengths larger than 400 nm to be incident. As shown in Fig. 5a, the photocurrents increase with bias potential for both n-SiNW/TiO_2 and n-Si/TiO_2, and the photocurrent of n-SiNW/TiO_2 is higher than that of n-Si/TiO_2 in the measuring potential region. When the bias potential is below 1.7 V (vs. SCE), neither samples show visible light photoresponse. When the bias potential exceeds 1.7 V (vs. SCE), the total photocurrent of n-Si/TiO_2 increases slowly and there is no visible light photoresponse. But the onset of the visible light photoresponse is observed at approximately 1.7 V (vs. SCE) for n-SiNW/TiO_2, whose total photocurrent increases accordantly with the visible light photocurrent. It is obvious that both UV light and visible light contribute the photocurrent, that is to say, n-SiNW/TiO_2 behave a window effect. Depending on window effect, the photocurrent of n-SiNW/TiO_2 reaches 1.44 mA cm^{-2} at 3.0 V (vs. SCE), which is 2.9-fold of that of n-Si/TiO_2 at the same potential. The SiNW/TiO_2 has the higher photocurrent density than the planar Si/TiO_2 due to high specific surface areas, enhanced antireflection ability, excellent transfer routes for charge carriers. The fact that Si/TiO_2 has no visible-light response is because TiO_2

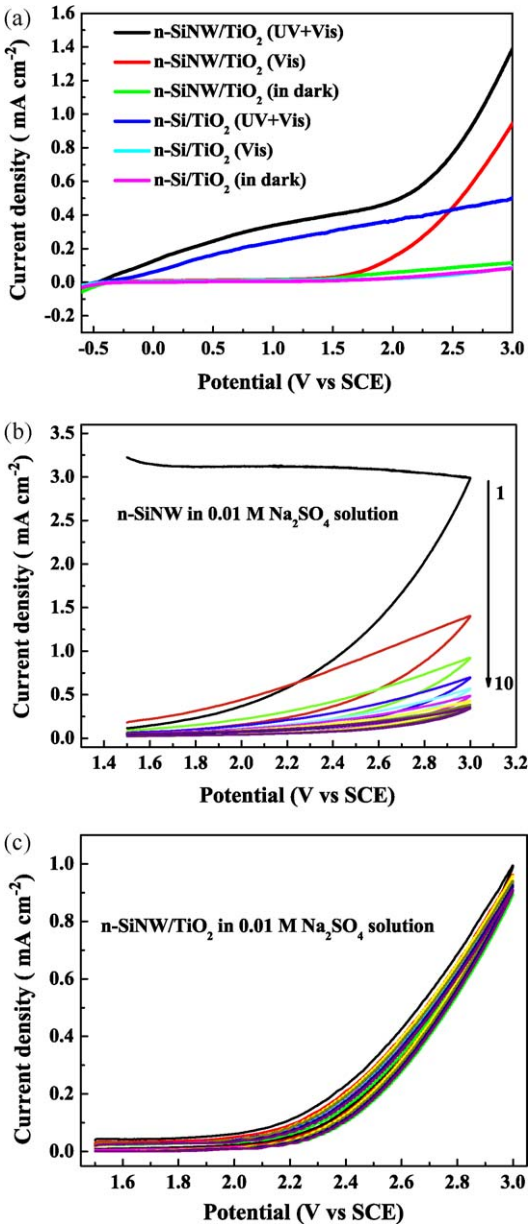

Fig. 5. (a) Photoelectrochemical properties of n-SiNW/TiO_2 in 0.01 M Na_2SO_4 solution under simulated solar light (UV + vis) and only visible light (vis). CV curves of n-SiNW (b) and n-SiNW/TiO_2 (c) in 0.01 M Na_2SO_4 solution under visible light.

layer on Si wafer surface is thicker than that around SiNW surface with the same deposition time. For a heterojunction with a planar film structure, there is an optimal thickness of the front semiconductor (wide band gap) [35]. If the thickness of TiO_2 layer on Si wafer exceeds the optimal thickness, the inner TiO_2 could not be induced and would obstruct the transfer of photogenerated carriers, and consequently, window effect would not occur.

In order to investigate the difference of visible light photoresponse between n-SiNW and n-SiNW/TiO_2 in solution, cyclic voltammetry (CV) characteristic was measured under visible light irradiation. According to the CV curves, the photocurrent of n-SiNW can not maintained constant in 0.01 M Na_2SO_4 solution (Fig. 5b). After 10 cycles, it decreases from above 3.0 mA cm^{-2} sharply to 0.34 mA cm^{-2} at 3.0 V (vs. SCE) and would decrease continuously. The photocurrent of n-SiNW/TiO_2, however, is steady and about 0.90 mA cm^{-2} after 10 cycles (Fig. 5c). These results indicate that the visible light photoresponse of n-SiNW/TiO_2 can be steady. Based on electrochemistry theory of

semiconductor, photocurrent could be generated when the n-Si anode is illuminated [36]. But this photocurrent is unstable in aqueous electrolytes [37]. In the electrolyte without fluoric anion, oxide would be generated on the surface of Si electrode and photocurrent would be shut off. Therefore, the photocurrent of SiNW itself is very large at the initial stage, and then decreasing gradually in general electrolyte. In the case of SiNW/TiO_2, SiNW could avoid the contact with the electrolyte duo to the TiO_2 layer existing, and no oxide of silicon could generate. As a result, the photocurrent could be maintained in the general electrolyte.

On the other hand, the oxidation of water is the only reaction under our experiment conditions. The anodic photocurrents are attributed to oxygen evolution, whose onset potential is about 2.1 V (vs. SCE), while the standard potential of oxygen evolution is 1.23 V (vs. NHE). Therefore, the overvoltage can be calculated to be about 1.1 V. Because water oxidation is a competing reaction in the photocatalytic degradation process of pollutant in aqueous solution, the high overvoltage of oxygen evolution is advantageous for pollutant oxidation [38,39].

The surface photovoltage (SPV) measurements are always used to observe the photoresponse abilities under different wavelengths because the signal of SPV is attributed to the changes of surface potential barriers before and after illumination [40]. In order to illuminate why n-SiNW/TiO_2 but n-Si/TiO_2 has window effect, the SPV spectra of n-Si, n-SiNW, n-Si/TiO_2 and n-SiNW/TiO_2 are shown in Fig. 6. The n-Si wafer exhibits photoresponse in all the wavelengths, and its SPV signal is obviously higher in visible light region from 400 to 800 nm than that in UV light region from 300 to 400 nm, which means that Si has preponderant photoresponse ability in visible light region. The SPV spectrum of n-SiNW is similar to that of n-Si, but its SPV signal is higher than n-Si possibly because of its excellent antireflection ability [41]. After deposition of TiO_2, which has main photoresponse in UV light region, SPV response of n-SiNW/TiO_2 is distinctly different from that of n-Si/TiO_2. In UV light region, both the SPV signals of n-Si/TiO_2 and n-SiNW/TiO_2 exhibit the characteristic of TiO_2. While in visible light region, no SPV response is observed from n-Si/TiO_2, but remarkable SPV response, which is similar to that of Si in shape, appears in case of n-SiNW/TiO_2. These phenomena illuminate that n-SiNW/TiO_2 can superpose the visible light photoresponse of n-SiNW and the UV light photoresponse of TiO_2, but n-Si/TiO_2 has no this ability. It is also noticed that the SPV signal of n-SiNW/TiO_2 is even higher than that of n-Si/TiO_2 in UV light region.

The type of SiNW/TiO_2 heterojunction can affect the behavior of window effect. Fig. 7 shows photocurrents of p-SiNW/TiO_2 and p-Si/TiO_2. Their photocurrents also increase with bias potential, and

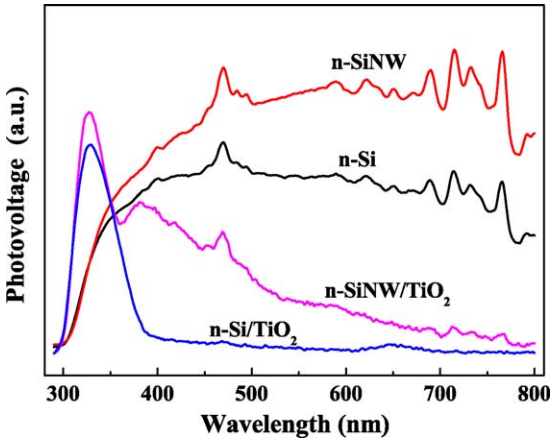

Fig. 6. SPV spectra of n-Si, n-SiNW, n-Si/TiO_2 and n-SiNW/TiO_2. (The data had been normalized.)

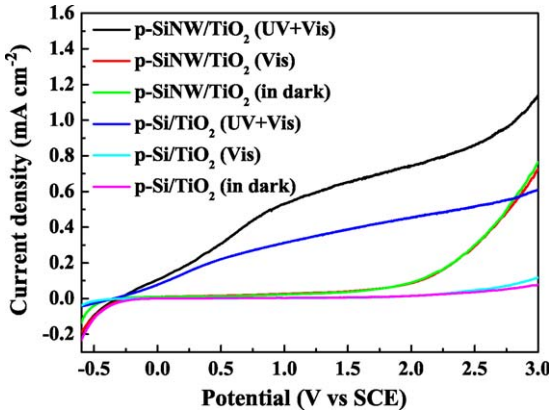

Fig. 7. Photoelectrochemical properties of p-SiNW/TiO_2 in 0.01 M Na_2SO_4 solution.

the photocurrent of p-SiNW/TiO_2 is higher than that of p-Si/TiO_2 in the measuring potential region. The abrupt increase of dark current is observed for potentials higher than 2.0 V (vs. SCE), and the visible light photocurrent curve is almost a repetition of dark current curve in the whole potential region, which illuminates p-SiNW/TiO_2 showing no visible light photoresponse.

3.3. Mechanisms

The extraordinary photoelectrochemical properties of SiNW/TiO_2 are illuminated by schematic band diagrams of the p-SiNW/TiO_2 and n-SiNW/TiO_2 heterojunctions as shown in Fig. 8. The diameter of SiNW in this paper is about 200 nm, which is too large to affect the energy bands [42], and therefore the energy bands of

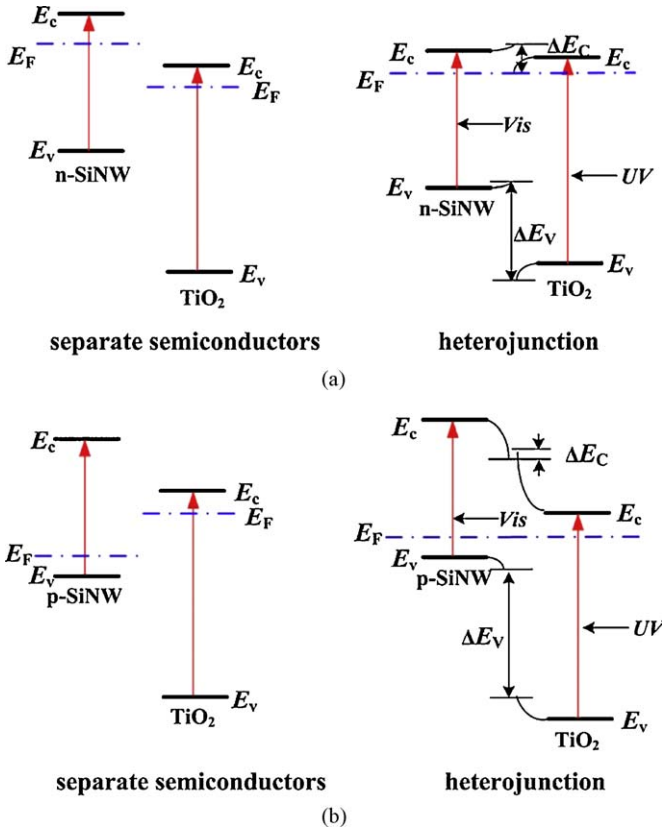

Fig. 8. Schematic band diagrams of separate semiconductors and after structuring heterojunction. (a) n-SiNW/TiO_2 and (b) p-SiNW/TiO_2.

SiNW are same to that of Si. The TiO_2 is a typical n-type semiconductor, whose Fermi level locates close to the conduction-band edge, which is more positive (vs. NHE) than that of n-SiNW. When TiO_2 nanoparticles are in contact with n-SiNW, the electrons will flow from the conduction band of n-SiNW into the conduction band of TiO_2 through the interface, and they will assemble in the TiO_2 side of the interface since electron is also the majority carriers for n-TiO_2 [43]. The flowing process will stop when the Fermi levels of the TiO_2 and n-SiNW are equal. In this process, the energy bands of n-SiNW shift downside with Fermi lever, whereas the energy bands of TiO_2 shift upside, leading to the valence band difference (ΔE_v) decreased. In fact, ΔE_v is the barrier for photogenerated-hole injection into TiO_2 from n-SiNW [44]. Once the applied voltage overcomes this barrier, the holes generated by visible light would transfer from n-SiNW to TiO_2, and participate in redox reactions together with the other holes generated from TiO_2 by UV light. As for p-SiNW, its Fermi level is more positive (vs. NHE) than that of TiO_2, the energy bands of p-SiNW and TiO_2 shift upside and downside, respectively, and the valence band difference (ΔE_v) should increase. Therefore, a big bias potential is required to overcome the valence band difference. But when the bias potential is higher than 2.0 V, which is still less than ΔE_v of p-SiNW/TiO_2, the dark current increases remarkably. Thus, the visible light photoresponse cannot be observed.

3.4. Photoelectrocatalytic activity

In order to evaluate the photoelectrocatalytic (PEC) ability of n-SiNW/TiO_2, the experiments of PEC degradation of phenol using n-Si/TiO_2 and n-SiNW/TiO_2 have been carried out. For comparison, phenol degradations in electrochemical process (EC) with n-SiNW/TiO_2 and directly photolytic process (DP) have been also performed. As shown in Fig. 9, under xenon lamp irradiation, in 3 h, the degradation efficiency of phenol in PEC is up to 99% involving n-SiNW/TiO_2, whereas it is 85% on n-Si/TiO_2. The PEC degradation of phenol follows pseudo-first-order kinetics, and the kinetic constants involving n-Si/TiO_2 and n-SiNW/TiO_2 are 0.010 (R^2 = 0.998) and 0.017 min^{-1} (R^2 = 0.998), respectively. The kinetic constant with the heterojunction arrays is 1.7 times as great as the value with the n-Si/TiO_2. To further illuminate the PEC ability of n-SiNW/TiO_2, the TOC is measured and the result is shown in Fig. 10. In 3 h, 66% of TOC are removed with n-SiNW/TiO_2 and only 33% with n-Si/TiO_2, respectively. The TOC removal of phenol on n-SiNW/TiO_2 is double to that on n-Si/TiO_2, indicating that considerable intermediate products are oxidized rapidly by n-SiNW/TiO_2 but accumulated in the solution using n-Si/TiO_2 (Fig. 11). The results confirm that n-SiNW/TiO_2 possesses higher mineralizing ability than n-Si/TiO_2.

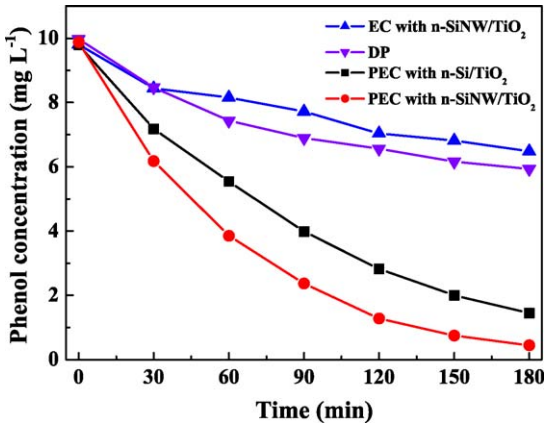

Fig. 9. EC, DP and PEC of solutions of phenol under xenon lamp irradiation (light intensity is 100 mW cm^{-2} and bias potential is 3.0 V vs. SCE).

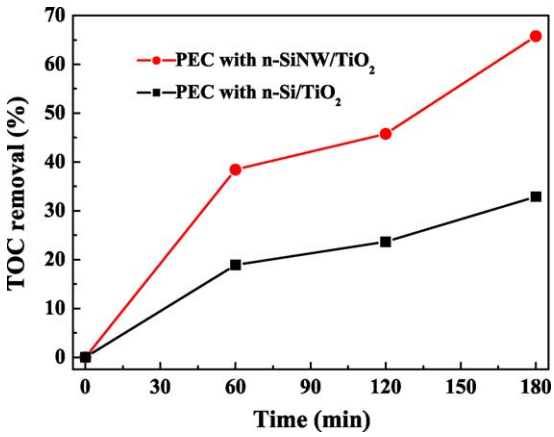

Fig. 10. Variation of TOC removal by PEC technology with n-Si/TiO_2 heterojunction arrays and n-SiNW/TiO_2 heterojunction arrays under xenon lamp irradiation (light intensity is 100 mW cm^{-2} and bias potential is 3.0 V vs. SCE).

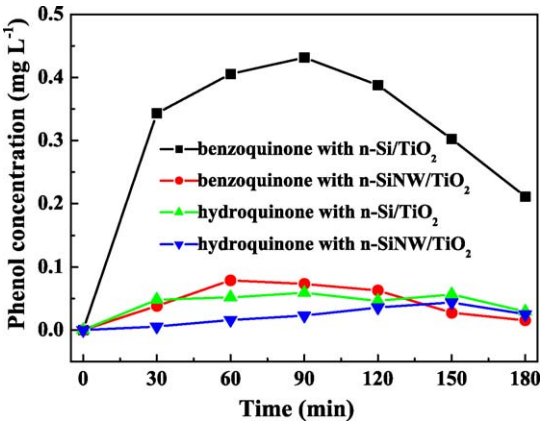

Fig. 11. Concentrations of intermediate products during the phenol degradation.

4. Conclusion

SiNW fabricated by chemical etching of Si wafer is a promising material to construct n–n and p–n heterojunctions with TiO_2. The heterojunction composed of n-type SiNW and TiO_2 possesses excellent photoconversion ability due to superposition of the UV light photoresponse of TiO_2 and the visible light photoresponse of SiNW. But the heterojunction of p-SiNW and TiO_2 has no this ability. The n-SiNW/TiO_2 heterojunction with window effect shows a higher mineralizing ability than n-Si/TiO_2. It is expected that this work would provide an access to synthesizing proper heterostructure for various application aims.

Acknowledgments

This work was supported by National Natural Science Foundation of China (No. 20837001) and the National Science Fund for Distinguished Young Scholars of China (No. 20525723).

Appendix A. Supplementary data

Supplementary data associated with this article can be found, in the online version, at doi:10.1016/j.apcatb.2009.03.010.

References

[1] U.I. Gaya, A.H. Abdullah, J. Photochem. Photobiol. C: Photochem. Rev. 9 (2008) 1–12.

[2] M.R. Hoffmann, S.T. Martin, W. Choi, D.W. Bahnemann, Chem. Rev. 95 (1995) 69–96.
[3] Y. Zhang, Jun. Li, J. Wang, Chem. Mater. 18 (2006) 2917–2923.
[4] P.C. Angelomé, L. Andrini, M.E. Calvo, F.G. Requejo, S.A. Bilmes, G.J.A.A. Soler-Illia, J. Phys. Chem. C 111 (2007) 10886–10893.
[5] L.M. Nikolic, L. Radonjic, V.V. Srdic, Ceram. Int. 31 (2005) 261–266.
[6] B. Huber, A. Brodyanski, M. Scheib, A. Orendorz, C. Ziegler, H. Gnaser, Thin Solid Films 472 (2005) 114–124.
[7] F.O. de Araújo, E.O. de Almeida, C. Alves Jr., J.A.P. da Costa, T. Dumelow, Surf. Coat. Technol. 201 (2006) 2990–2993.
[8] A. Kolouch, P. Hájková, A. Macková, M. Horáková, J. Houdková, P. Špatenka, S. Hucek, Plasma Process. Polym. 4 (2007) S350–S355.
[9] K. Wang, B. Yao, M.A. Morris, J.D. Holmes, Chem. Mater. 17 (2005) 4825–4831.
[10] I. Oja, A. Mere, M. Krunks, R. Nisumaa, C.H. Solterbeck, Thin Solid Films 515 (2006) 674–677.
[11] B. Karunagaran, S.J. Chung, E.K. Suh, D. Mangalaraj, Physica B 369 (2005) 129–134.
[12] J. Domaradzki, K. Nitsch, Thin Solid Films 515 (2007) 3745–3752.
[13] J.W. Gerlach, S. Mändl, Nucl. Instrum. Meth. B 242 (2006) 289–292.
[14] S. Liang, M. Chen, Q. Xue, Z. Liu, Thin Solid Films 516 (2008) 3058–3061.
[15] B. Vallejo, M. Gonzalez-Mañas, J. Martínez-López, F. Morales, M.A. Caballero, Sol. Energ. Mater. Sol. Cell 86 (2005) 299–308.
[16] V. Siriwongrungson, M.M. Alkaisi, S.P. Krumdieck, Surf. Coat. Technol. 201 (2007) 8944–8949.
[17] Q. Wu, D. Li, Z. Chen, X. Fu, Photochem. Photobiol. Sci. 5 (2006) 653–655.
[18] C.Y. Lin, Y.K. Fang, C.H. Kuo, S.F. Chen, C. Lin, T.H. Chou, Y. Lee, J. Lin, S. Hwang, Appl. Surf. Sci. 253 (2006) 898–903.
[19] H. Yu, X. Quan, S. Chen, H. Zhao, Y. Zhang, J. Photochem. Photobiol. A: Chem. 200 (2008) 301–306.
[20] H. Chen, S. Chen, X. Quan, H. Yu, H. Zhao, Y. Zhang, J. Phys. Chem. C 112 (2008) 9285–9290.
[21] K. Peng, Y. Yan, S. Gao, J. Zhu, Adv. Funct. Mater. 13 (2003) 127–132.
[22] E.C. Garnett, P. Yang, J. Am. Chem. Soc. 130 (2008) 9224–9225.
[23] Y. Cui, X. Duan, J. Hu, C.M. Lieber, J. Phys. Chem. B 104 (2000) 5213–5216.
[24] L. Yu, Physics of Semiconductor Heterojunctions (Chinese edition), 2nd ed., Science Press, Beijing, 2006, 247 pp.
[25] J.Y. Kim, K. Lee, N.E. Coates, D. Moses, T.Q. Nguyen, M. Dante, A.J. Heeger, Science 317 (2007) 222–225.
[26] K.S. Lim, M. Konagai, K. Takahashi, J. Appl. Phys. 56 (1984) 538–542.
[27] O. Hagemann, M. Bjerring, N.Chr. Nielsen, F.C. Krebs, Sol. Energ. Mater. Sol. Cell 92 (2008) 1327–1335.
[28] Y. Hu, Z. Zheng, H. Jia, Y. Tang, L. Zhang, J. Phys. Chem. C 112 (2008) 13037–13042.
[29] S.S. Kale, R.S. Mane, T. Ganesh, B.N. Pawar, S.H. Han, Curr. Appl. Phys. 9 (2009) 384–389.
[30] W. Siripala, A. Ivanovskaya, T.F. Jaramillo, S.H. Baeck, E.W. McFarland, Sol. Energ. Mater. Sol. Cell 77 (2003) 229–237.
[31] E.L. Miller, B. Marsen, D. Paluselli, R. Rocheleau, Electrochem. Solid-State Lett. 8 (2005) A247–A249.
[32] A.H. Jahagirdar, N.G. Dhere, Sol. Energ. Mater. Sol. Cell 91 (2007) 1488–1491.
[33] A. Goetzberger, C. Hebling, H.W. Schock, Mater. Sci. Eng. R 40 (2003) 1–46.
[34] A. Weibel, R. Bouchet, F. Boulc'h, P. Knauth, Chem. Mater. 17 (2005) 2378–2385.
[35] S. Hinckley, J.F. McCann, D. Haneman, Sol. Cells 17 (1986) 317–342.
[36] V. Lehmann, H. Foll, J. Electrochem. Soc. 135 (1988) 2831–2835.
[37] Y. Nakato, T. Ueda, Y. Egi, H. Tsubomura, J. Electrochem. Soc. 134 (1987) 353–358.
[38] B. Marselli, J. Garcia-Gomez, P.A. Michaud, M.A. Rodrigo, Ch. Comninellis, J. Electrochem. Soc. 150 (2003) D79–D83.
[39] N.B. Tahar, A. Savall, J. Electrochem. Soc. 145 (1998) 3427–3434.
[40] L. Kronik, Y. Shapira, Surf. Sci. Rep. 37 (1999) 1–206.
[41] K. Peng, Y. Wu, H. Fang, X. Zhong, Y. Xu, J. Zhu, Angew. Chem. Int. Ed. 44 (2005) 2737–2742.
[42] J.A. Yan, L. Yang, M.Y. Chou, Phys. Rev. B 76 (2007) 115319.
[43] S.I. Cserveny, Int. J. Electronics 25 (1968) 65–80.
[44] C.C. Fulton, G. Lucovsky, R.J. Nemanich, Appl. Phys. Lett. 84 (2004) 580–582.